

Responses to Reviewer #3 (report #2).

1) Figure A would be a nice supporting evidence to add.

Reply: Agree. We have included it as Fig. 4 and added some explanations in lines 168-171.

2) The authors misunderstood my specific comment 1). The problem with “soil water” and “soil water redistribution” is not with “water”, but with “soil” and “redistribution”. In this study, the flow that is being simulated with the new parameterization is not of “soil water” per se, because it has not mixed with soil yet. It is a bulk flow within the root channel. “Soil water/moisture redistribution” implies that water gets mixed with soil in one particular place, and then gets picked up somehow to be re-deposited to another place. That’s not what is happening in this study. Maybe change the sentence to “.... in the form of bulk flow through the stem-root flow mechanism ...”?

Reply: Now we get it. The point is well taken. We have modified the first sentence in the abstract accordingly as “Rainfall that reaches the soil surface can rapidly move into deeper layers in the form of bulk flow through the stem-root flow mechanism.”

Stem-root flow effect on soil-atmosphere interactions and uncertainty assessments

Tzu-Hsien Kuo¹, Jen-Ping Chen¹, and Yongkang Xue²

¹ Department of Atmospheric Sciences, National Taiwan University, Taipei, Taiwan, R.O.C.

² Department of Atmospheric and Oceanic Sciences, and Department of Geography,
University of California, Los Angeles, California, U.S.A.

* Corresponding Author:

Jen-Ping Chen, Professor

Department of Atmospheric Sciences, National Taiwan University

No. 1, Sect. 4, Roosevelt Road, Taipei, Taiwan 10673

Email: jpchen@as.ntu.edu.tw

Phone: +886-2-33663912; Fax: +886-2-23633317

Abstract

Rainfall that reaches the soil surface can rapidly move into deeper layers in the form of bulk flow through the stem-root flow mechanism. This study develops the stem-root flow parameterization scheme and coupled this scheme with the Simplified Simple Biosphere model (SSiB) to analyze its effects on land-atmospheric interactions. The SSiB model was tested in a single column mode using the Lien Hua Chih (LHC) measurements conducted in Taiwan and HAPEX-Mobilhy (HAPEX) measurements in France. The results show that stem-root flow generally caused a decrease in soil moisture at the top soil layer and moistened the deeper soil layers. Such soil moisture redistribution results in substantial changes in heat flux exchange between land and atmosphere. In the humid environment at LHC, the stem-root flow effect on transpiration was minimal, and the main influence on energy flux was through reduced soil evaporation that led to higher soil temperature and greater sensible heat flux. In the Mediterranean environment of HAPEX, the stem-root flow substantially affected plant transpiration and soil evaporation, as well as associated changes in canopy and soil temperatures. However, the effect on transpiration could be either positive or negative depending on the relative changes in the soil moisture of the top soil versus deeper soil layers due to stem-root flow and soil moisture diffusion processes.

删除: via vertical redistribution of soil moisture

18 Key words: stemflow, root flow, soil moisture, evapotranspiration, land-atmospheric interaction, SSIB

22 1. Introduction

23 The water stored in the land system is a key factor controlling many physical processes and
24 feedback between the land and atmosphere. Soil moisture is a source of water for the atmosphere
25 through processes that lead to evapotranspiration, including bare soil evaporation, plant transpiration
26 and evaporation from other surfaces such as leaves, snow, etc. The rainfall redistribution process in
27 forest systems affects soil moisture amount and its distribution (McGuffie et al., 1995; Chase et al.,
28 1996; Chase et al., 2000; Zhao et al., 2001). Rain water entering the forest is redistributed via
29 several pathways before reaching the forest floor, e.g., some is intercepted by the canopy and some
30 reaches the soil as throughfall. A significant amount of rainwater intercepted by the canopy can flow
31 down along tree stems and reach the forest floor in a process termed stemflow. The efficiency of
32 stemflow varies with plant species, seasons, meteorological conditions, rainfall intensity, and canopy
33 structure (Levia and Frost, 2003; Levia and Germer, 2015). Johnson and Lehmann (2006)
34 summarized various field measurements and showed that the fraction of precipitation that becomes
35 stemflow ranges from 0.07% to 22%.

36 In contrast to the throughfall that infiltrates slowly through the top soil, stemflow can continue via
37 the root system (hereafter called the “stem-root flow”) and quickly reach deep soil layers and the water
38 table (Liang et al., 2007; 2009). It has long been recognized that the stem-root flow can help to store
39 water in deeper soil layers and thus create favorable conditions for plant growth under arid conditions
40 (Návar, 1993; Li et al., 2009). Soil moisture redistribution by stem-root flow not only affects

41 vegetation growth but also land evapotranspiration and runoff (Neave and Abrahams, 2002).
42 Furthermore, the enhanced water penetration can significantly alter groundwater recharge. Taniguchi
43 et al. (1996) showed that in a pine forest, the stem-root flow contributed approximately 10–20% of
44 annual groundwater recharge even with a stemflow-to-precipitation ratio of only 1%.

45 Stem-root flow effects have not been considered in most land-surface schemes of climate models.
46 Tanaka et al. (1996) developed a model to evaluate the effect of stem-root flow on groundwater. This
47 model is yet to be implemented in current land surface models. Li et al. (2012) pointed out that
48 stemflow hydrology and preferential flow along roots are intimately linked, but direct integration of
49 these processes into land models, to our knowledge, has not been reported.

50 In this paper, we parameterized the stem-root flow processes in a land surface model named the
51 Simplified Simple Biosphere Model (SSiB; Xue et al., 1991), and analyzed how stem-root flow affects
52 soil moisture and whether this effect is significant enough to influence atmospheric processes. Soil
53 moisture data from two sites, located at Lien Hua Chih, Taiwan (LHC) and Bordeaux/Toulouse, France
54 (from the HAPEX-Mobilhy experiment, hereafter called HAPEX), were collected for model
55 evaluation. The two sites represent different climate regimes and terrestrial ecosystem, and stem-root
56 flow modifies their surface energy and water processes in somewhat dissimilar ways.

57

58 2. Methodology

59 2.1 The stem-root flow model

60 In the original SSiB land surface model (Xue et al., 1996), vertical soil moisture movement is

61 described by the diffusion equations:

$$\begin{aligned} \frac{\partial \theta_1}{\partial t} &= \frac{1}{D_1} [P + Q_{12} - E_{SE} - b_1 E_{TR,1}] \\ 62 \quad \frac{\partial \theta_2}{\partial t} &= \frac{1}{D_2} [-Q_{12} + Q_{23} - b_2 E_{TR,2}] \\ \frac{\partial \theta_3}{\partial t} &= \frac{1}{D_3} [-Q_{23} + Q_3 - b_3 E_{TR,3}] \end{aligned} \quad (1)$$

63 where the subscripts 1, 2 and 3 are indices of the top, middle, and bottom soil layers, respectively; θ is

64 the soil moisture content, expressed as a fraction of the saturated value; D is soil thickness; P is

65 effective precipitation flux on the soil surface, composed of the direct throughfall and the throughfall

66 from leave-intercepted rainfall (cf. Fig. 1); $Q_{ij} = -k[\partial\Psi/\partial z + 1]$ is the flux of water between the i^{th}

67 and j^{th} layers, and is defined to be positive in an upward direction; Ψ (in m) is the soil water potential;

68 E_{SE} is the evaporation rate of bare soil; i is the soil layer index; $E_{TR,i}$ is the transpiration rate in soil

69 layer; b_i is the proportionality factor that accounts for root distribution; Q_3 is the water flux entering the

70 water table. The similar approach has been used by many land surface models. Note that the middle

71 soil layer can be divided into more sublayers with similar formula as used for the middle layer. In

72 these equations, the transfer velocity Q_{ij} considers only the soil diffusion flow. This study develops

73 the parameterizations that include the stem-root flow mechanism which provides a “bypass” for water

74 to channel through the soil on root surfaces (Fig. 1). The stemflow reaching the top soil layer, q_0 , is

75 often represented as a fraction of the total precipitation (or, more precisely, the leaf drainage) such that

76 direct rainfall entering the soil becomes

$$77 \quad P' \equiv P - q_0. \quad (2)$$

78 By relating the stemflow to leaf drainage, there is an implicit threshold for stemflow initiation that
 79 corresponding to the threshold of leaf drainage.

80 After entering the soil, the root flow is divided into a downward transfer flux q_z (within the root
 81 system) and a lateral transfer flux q_x (from the root surface to the soil). These two fluxes can be
 82 parameterized as following:

$$83 \quad q_{z,i} = \alpha_z A_i h_i V_s \quad (3)$$

$$84 \quad q_{x,i} = \begin{cases} \alpha_x R_i A_i K(\Psi_i) \left(\frac{\Psi_i - \Psi_s}{D_{\text{eff}}} \right), & \text{if } h_i > 0 \\ 0, & \text{if } h_i = 0 \end{cases} \quad (4)$$

85 where α_z and α_x are proportionality coefficients; A_i (in $\text{m}^2 \text{m}^{-3}$) is the total root surface area density that
 86 varies with vegetation types (Böhm, 1979; Zhang et al., 2005; Li et al., 2013); h_i (in m) is the thickness
 87 of water on the root surface; V_s (in m s^{-1}) is the terminal velocity of root flow; R_i (in m) is the root
 88 length; K (in m s^{-1}) is the hydraulic conductivity of the soil; Ψ_s (in m) is the soil water potential at
 89 saturation; Ψ_i (in m) is the soil water potential; and D_{eff} (in m) is the effective thickness of the
 90 water-soil interface. Derivation of D_{eff} is described in the appendix. Due to a lack of observational
 91 data, we used a vertically uniform root distribution. However, different root depths were used based
 92 on the measurements (100 cm for LHC and 140 cm for HAPEX). Note that $q_0 = q_{x,1} + q_{z,1}$
 93 according to the mass conservation principle. From Eqs. (1), (2), and (4), we have:

$$94 \quad \begin{aligned} \frac{\partial \theta_1}{\partial t} &= \frac{1}{D_1} [P' + Q_{12} - E_{SE} - b_1 E_{TR,1} + q_{x,1}] \\ \frac{\partial \theta_2}{\partial t} &= \frac{1}{D_2} [-Q_{12} + Q_{23} - b_2 E_{TR,2} + q_{x,2}] \\ \frac{\partial \theta_3}{\partial t} &= \frac{1}{D_3} [-Q_{23} + Q_3 - b_3 E_{TR,3} + q_{x,3}] \end{aligned} \quad (5)$$

95 The changes in root surface water thickness h_i obey the mass conservation principle and thus are

96 controlled by the vertical and horizontal fluxes of root flow. Its tendency can be described as:

$$97 \quad \frac{dh_i}{dt} = \begin{cases} \frac{(q_{z,i-1} - q_{z,i} - q_{x,i})}{A_i R_i}, & \text{if } h_i > 0 \\ 0, & \text{if } h_i = 0 \end{cases} \quad (6)$$

98 Equations (5) and (6) represent the water budgets in the soil and root flow systems, respectively, and

99 they are linked through the term q_x in Eq. (4).

100 Stemflow input into the first soil layer (q_0) is represented as a fraction of the leaf drainage (LD),

101 which is the portion of precipitation that is intercepted by the canopy minus leaf evaporation and can

102 be calculated in SSiB. LD is similar to canopy drip in some other models, and is represented mainly

103 as a function of the leaf area index (LAI). The ratio of q_0 to LD depends mainly on plant type, as well

104 as meteorological conditions such as wind speed (Levia and Frost, 2003; Johnson and Lehmann, 2006;

105 André et al., 2008; Siegert and Levia, 2014). Unfortunately, there is still insufficient information to

106 determine the ratio of q_0 and LD. We conducted a series of sensitivity tests with systematically

107 varying ratio between the q_0 to LD to assess the uncertainty.

108 The stem-root flow parameterization was tested using the offline SSiB, which is a simplified

109 version of the land-biosphere model developed by Sellers et al. (1986). The model recognizes 12

110 different vegetation types according to Dorman and Sellers (1989), and is set up with 3 soil layers and

111 1 canopy layer. The SSiB model has 8 prognostic variables: soil wetness for 3 layers; temperature at

112 the canopy, ground surface and deep soil layers; snow depth at ground level; and water intercepted by

113 the canopy. An additional variable – h_i – was added for each soil layer to account for the stem-root

114 flow mechanism. An implicit backward scheme was used to calculate the temperature tendency in the
115 coupling of the lowest atmospheric model layer with SSiB, such that energy conservation between the
116 land surface and the atmosphere was satisfied. Soil temperature was calculated using the
117 force-restore method, and water movement in the soil was described by the diffusion equation as
118 shown in Eq. (5).

119 Following typical offline simulation procedures for single-column land surface model, in situ
120 atmospheric data were applied to drive the SSiB model in 30 min time resolution. These specified
121 variables include pressure, temperature, humidity, wind speed, net radiation and rainfall. Soil
122 conditions were initialized with each site's measurement data. The spin up time for coupled land
123 surface model typically ranges from a couple of months to over a year, but can be shorter when
124 running in off-line (single column) mode and with good initial soil conditions (de Goncalves et al.,
125 2006; Yang et al., 2011; Lim et al., 2012; Angevine et al., 2014). Our simulations applied
126 measurement data for model initialization, and the results show that the soil conditions reached
127 physical balance within a few weeks. So, at the last 10 months results of our simulations are
128 reliable.

129 2.2 Experimental design and site information

130 Two sites with different climate and vegetation conditions were selected to test the stem-root flow
131 parameterizations in the SSiB model. The first is a site with warm-to-temperate mountain rainforest
132 condition from the Lien Hua Chi (LHC; 23°55'N, 120°53'E), Taiwan. LHC is located in the Central

133 Mountain Range of Taiwan, with a hilly terrain and a mean altitude of 770 m above sea level in the
134 surroundings. The average annual rainfall at LHC is 2317 mm, with rain falling predominantly in late
135 summer and early autumn (Fig. 2). With ample rainfall, LHC is covered with dense forest with an
136 average canopy height of approximately 17 m. The vegetation cover is comprised of mixed
137 evergreens and hardwood species, including *Cryptocarya chinensis*, *Engelhardtia roxburghiana*,
138 *Tutcheria shinkoensis*, and *Helicia formosana*. The soil has a loamy texture with an average bulk
139 density of 1.29 g cm^{-3} and a porosity of 0.53 over the top 1.0 m (Chen, 2012). Soil moisture
140 measurements were collected at depths of 10, 30, 50, 70 and 90 cm.

141 The second is the HAPEX-Mobilhy data collected at the Caumont site (SAMER station No. 3;
142 $43^{\circ}41' \text{N}$, $0^{\circ}6' \text{W}$) with an elevation of 113 m above sea level and relatively flat terrain. This site has a
143 Mediterranean climate, with an annual rainfall of 856 mm, most of which occurs in spring and winter
144 (Fig. 3). In contrast to the LHC site with dense forest, the HAPEX site is covered mostly with short
145 and sparse soya crops, and the surface albedo stays nearly constant at 0.20 throughout the year
146 (Goutorbe et al., 1989). The soil type is mainly silt, mixed with sand and clay (see Table 1). Soil
147 moisture content was measured every 10 cm from the surface to a depth of 1.6 m using neutron
148 sounding probes on a weekly basis (Goutorbe, 1991; Goutorbe and Tarrieu, 1991). Note that the
149 HAPEX data have higher vertical resolution in the soil column but lower temporal resolution
150 compared with the LHC data. To simplify comparisons, the soil moisture data were converted into
151 three vertical layers. For the HAPEX data, the top (SM1), middle (SM2) and bottom (SM3) layers

152 correspond to the 0–20 cm, 20–50 cm, and 50–150 cm depths, respectively. For LHC, SM1
153 corresponds to a depth of 10 cm, SM2 is the average of the 30 cm and 50 cm soil layers, and SM3
154 corresponds to a depth of 90 cm.

155 Figures 2 and 3 show the seasonal variations of precipitation and soil moisture at different depths.
156 It is generally expected that soil moisture response to rainfall should be faster in the upper than in the
157 lower layers. However, the LHC measurements (Fig. 2) showed that the soil moisture fluctuation was
158 stronger in the middle layer than in the upper layer during the dry season when the soil moisture was
159 not saturated. Fluctuations were not obvious in rainy seasons when SM2 and SM3 are almost
160 saturated. This phenomenon is likely an indication of the preferential flow due to the root flow
161 mechanism. This phenomena, however, was not observed in the HAPEX data (Fig. 3), which may be
162 due to the coarse temporal resolution (weekly) of the data or a weaker root flow effect from the soya
163 crop, and the latter will be discussed later. [Figure 4 shows the correlation between hourly changes in](#)
164 [precipitation and soil moisture at LHC in 2010. The correlations are higher at deeper layers and](#)
165 [during stronger rainfall intensities. Such a relationship is a good indication of the stem-root flow](#)
166 [mechanism.](#)

167 To test the response of soil moisture to precipitation in these two sites using the modified SSiB
168 model, a set of parameters have to be selected. These include the soil and terrain properties listed in
169 Table 1, as well as the monthly LAI coefficients in Table 2. In addition, some parameters in Eqs.
170 (3)–(6) have to be decided. Two required but little-known parameters are the root-flow velocity V_s

171 and the stemflow to leaf drainage ratio (SLR; i.e., q_0/LD). The root-flow velocity V_s is related to root
172 structure and soil texture, but such information is very limited. Studies have indicated that water flow
173 in the root-channel is approximately 100 times higher than the soil diffusion flow (Beven and Germann,
174 1982; Liu et al., 1994; Jarvis and Dubus, 2006; Köhne et al., 2009; Gerke, 2014). The maximum soil
175 diffusion flow can be represented by the saturated hydraulic conductivity, which was measured as
176 $4 \times 10^{-6} \text{ m s}^{-1}$ at HAPEX and $1 \times 10^{-6} \text{ m s}^{-1}$ at LHC. Therefore, we set the root-flow velocity V_s as
177 10^{-4} m s^{-1} in the simulation, and will discuss the associated uncertainty later.

178 The SLR value depends on a number of parameters as discussed in the previous section. This
179 study evaluated SLR-introduced uncertainty by conducting sensitivity tests with systematically
180 varying SLR from 0 to 100%, and identified optimal value that yielded the best soil moisture profiles
181 compared with the observations. The optimal SLR value for the HAPEX experiment was
182 approximately 50%, compared with 90% for the LHC case. These values reflect the large contrast in
183 leaf coverage and plant type between the two sites. In these experiments, we set A_i to $0.5 \text{ m}^2 \text{ m}^{-3}$
184 based on the Li et al. (2013) and the proportionality coefficients, α_z and α_x , are set to 1. The
185 uncertainty discussion for V_s and SLR should include the uncertainty caused by these parameters.
186 When more observational data are available, we could revisit these issues further. All simulations
187 used integration time step of 30 minutes.

188

189 3. Effect of stem-root flow on soil moisture

190 The modified SSiB model was used to simulate the intra-annual variations in soil conditions for
191 the 2010 LHC case and the 1986 HAPEX case. For the LHC case, the simulation well captured the
192 soil moisture increase associated with precipitation events followed by rapid drying (Fig. 5). Changes
193 in SM1, SM2 and SM3 all reached the 95% confidence level in all seasons. In many instances, the
194 simulated soil moisture fluctuation was stronger in the middle layer than in the top or bottom layers, as
195 found in the observations. The shading shows the range of values enclosed by the two extremes of
196 SLR (i.e., 0% and 100%). Results with other SLR ratios (not shown) generally lie within these limits
197 but may occasionally fall out of bound, indicating some nonlinearities. When SLR is zero, which has
198 no stem flow effect and is referred to as the control run in this paper, the soil moisture of the middle
199 layer is very low and fluctuates less in response to rainfall events (Fig. 5). The simulation generally
200 underestimated the soil moisture in the bottom layer even with the root-flow mechanism. In the top
201 layer, the model overestimated soil moisture in spring and winter, but underestimated it during autumn.
202 Such discrepancies are generally less substantial when the stem-root flow mechanism is included, as
203 indicated by the generally lower bias and root-mean-square error shown in Table 3. The possible
204 causes of error will be elaborated in the discussion section.

205 For the HAPEX case, the simulations also well captured the seasonal cycle as well as the sharp
206 fluctuations in the top layer (Fig. 6). The responses of SM2 and SM3 to the stem-root flow are
207 statistically significant (>95% confidence) during late summer and autumn (the main growing season
208 and relatively dry soil); whereas the responses in SM1 reached only 94% confidence level. Without

刪除: 4

刪除: 4

刪除: 5

212 the stem-root flow mechanism, soil moisture was generally overestimated in the two upper layers and
213 underestimated in the bottom layer, except during April and May when all layers were too dry. When
214 stem-root flow with SLR=50% was considered, the model performed better in all layers (see Table 3).
215 Stem-root flow with a much higher SLR (e.g., SLR=100%) produced worse results for soil moisture in
216 the surface and middle layers. Note that SLR=50% produced the driest middle layer, indicating that
217 the stem-root flow effect is nonlinear because both stem-root flow and diffusion, as well as their
218 interactions, play role in soil moisture variations. Note that SSiB does not consider the potential role
219 of plant uptake, which might be potentially important in the middle layer. In the bottom layer, more
220 accurate soil moisture was obtained with SLR=100%, but this does not necessarily mean that the
221 stem-root flow was underestimated. The overestimation of soil moisture in SM1 and the
222 underestimation in SM3 in spring may be coupled, due to mechanisms that are missing in our model.
223 This issue will be elaborated in the discussion section.

224 It is also worth mentioning that both the observation and simulation showed weaker soil moisture
225 fluctuations in the middle than in the surface layer, a feature very different from the LHC case. It is
226 likely that there is a weaker stem-root flow associated with plant and soil types in the HAPEX case.

227 Figures 5 and 6 demonstrate that the strength of the stem-root flow is greater in LHC, with associated
228 changes in soil moisture of up to $0.1 \text{ m}^3 \text{ m}^{-3}$ compared with the maximum changes of $0.05 \text{ m}^3 \text{ m}^{-3}$ at
229 HAPEX. This is simply because LHC has more intense rainfall than HAPEX.

230

刪除: 4

刪除: 5

233 4. Effect of stem-root flow on energy flux

234 The results in last section show that stem-root flow can alter the vertical profile of soil moisture.

235 It is important to know whether such a modification has significant effects on evapotranspiration and

236 associated interactions between the land and atmosphere. The soil moisture in the top soil layer in the

237 LHC case generally decreased due to stem-root flow, except in some instances (e.g., mid-September,

238 the later dry season) when the enhanced moisture storage in the deep layers replenish the moisture in

239 the drying surface soil through moisture diffusion. The changes in plant transpiration, however, were

240 insignificant (red curve in Fig. 7a), as this process is associated with soil moisture not only in the top

刪除: 6

241 layer but also in the deeper layers that are within the reach of the root system. Therefore, the effect of

242 surface layer drying on transpiration may be compensated by the moistening of the lower layers. Soil

243 moisture in these layers are well above the wilting point to support the normal transpiration.

244 Meanwhile, the drying of the surface soil resulted in less soil evaporation (Fig. 7a), which heavily

刪除: 6

245 relies on soil moisture near soil surface, and thus weaker the total latent heat release (see Table 4 for the

246 mean and maximum changes in daily temperatures and energy fluxes). This led to a higher soil

247 surface temperature and consequently stronger sensible heat flux (blue curve in Fig. 7b), which

刪除: 6

248 resulted in warmer air (magenta curve in Fig. 8b) and thus stronger rainwater evaporation from the leaf

刪除: 7

249 surface (green curve in Fig. 7a).

刪除: 6

250 In the HAPEX case, the stem-root flow caused a general drying of the top soil, except for a brief

251 period in mid-October (Fig. 8a). However, responses in soil evaporation were not as straightforward

刪除: 7

258 as in the LHC case. For example, in late July (just after the start of the growing season) there was a
259 spike in the evaporation but a reduction in the moisture of the top soil layer (blue curve in Fig. 8a). As
260 wind speed is the same for both cases, the increase in soil evaporation must be due to either a higher
261 soil temperature and/or a lower water vapor density in the air near the soil surface. This was indeed
262 the case (magenta and black curves in Fig. 8b) and found to be driven by changes in transpiration.

刪除: 7

263 Soil moisture in the HAPEX case was generally much lower than in the LHC case and
264 occasionally fell below the wilting point. The stomatal resistance that controls transpiration is very
265 sensitive to the soil moisture near the wilting point. As such, a slight decrease in the moisture of the
266 top soil layer can dramatically reduce transpiration. When soil moisture approached the wilting point

267 in late July, plant transpiration reduced sharply in response to the stem-root flow effect (red curve in

268 Fig. 8a). Such a change in plant transpiration caused an increase in the air temperature near the soil

刪除: 7

269 surface (magenta curve in Fig. 8b) and a decrease in air humidity, which increased soil evaporation

刪除: 7

270 (blue curve in Fig. 8a). In early August, however, soil moisture accumulated in the bottom layer

刪除: 7

271 through the stem-root flow (cf. Fig. 6c) and the stomatal resistance began to decrease such that

刪除: 5

272 transpiration recovered and soon dominated the overall evapotranspiration throughout the rest of the

273 growing season. The increased transpiration also caused a reduction in air temperature and surface

274 temperature and thus the associated sensible heat flux (blue curve in Fig. 8b). During late August to

刪除: 7

275 mid-September, surface soil moisture was so low in some instances (cf. Fig. 6a), transpiration was

刪除: 5

276 shutdown with or without the stem-root flow effect. In these instances, the net energy flux was

285 controlled by soil evaporation (Fig 8b).

刪除: 7

286

287 5. Discussion

288 The above analyses indicate that stem-root flow affects the energy flux mainly through changing
289 the balance between surface soil evaporation and sensible heat fluxes in the humid environment of
290 LHC, and through changing plant transpiration and sensible heat fluxes over the relatively dry
291 environment at HAPEX. The associated changes in annual energy flux to the atmosphere are strongly
292 positive at LHC, but nearly balanced at HAPEX. However, the magnitude of the changes of the
293 individual energy flux component was significantly higher for HAPEX (peaked at approximately -67
294 and +51 W m⁻² for transpiration and sensible heat, respectively) than for LHC (peaked at
295 approximately -16 and +31 W m⁻² for evaporation and sensible heat, respectively) due to its drier
296 Mediterranean environment.

297 Another interesting contrast between the two cases is the relationship between sensible heat and
298 total heat (sensible heat plus latent heat). In the LHC case, the responses of sensible heat and total

299 heat to the stem-root flow are generally of the same sign (Fig. 7b), whereas they have opposite signs in

刪除: 6

300 the HAPEX case (Fig. 8b). Furthermore, the net change in heat flux is dominated by sensible heat at

刪除: 7

301 LHC but by latent heat at HAPEX. Budyko (1974) proposed two main evapotranspiration regimes:
302 soil moisture-limited and energy-limited. As summarized by Seneviratne et al. (2010), when soil
303 moisture remains above a critical value, the fraction of evapotranspiration of the total energy flux is

307 independent of the soil moisture content (energy-limited regime); below the critical soil moisture value,
308 the soil moisture content provides a first-order constraint on evapotranspiration (soil moisture-limited
309 regime). Therefore, the evapotranspiration responses to the stem-root flow as discussed above imply
310 that HAPEX is in the soil moisture-limited regime, whereas LHC is in the energy-limited regime.
311 Note that this regime separation needs to take into account the contribution of deep soil moisture to
312 transpiration.

313 Regarding the partition of water transport, recent studies (e.g., Jasechko et al., 2013; Good et al.,
314 2015; Wei et al., 2015) explored the dominant role of transpiration in ecosystem evapotranspiration.
315 The results of this work partially concur with these studies. In other words, the stem-root flow in the
316 plant-soil system could enhance the transpiration, and reduce the soil evaporation, which regulated the
317 partition of evapotranspiration. A number of PILPS studies, including the PILPS-HAPEX
318 experiment (Boone and Wetzel, 1996; Henderson-Sellers, 1995; Shao et al., 1996; Xue et al., 1996)
319 consistently demonstrated that the current land model parameterizations have the weakness in
320 simulating the soil moisture in the dry season. This study by introducing a parameterization on the
321 stem-root flow mechanisms, wish to help solve this deficiency. With the stem-root flow mechanism,
322 the soil moisture will redistribute in vertical, leading to better simulated results in each layer, which
323 is important for the evapotranspiration partition.

324 By including the stem-root flow mechanism, the land surface model appears to better simulate the
325 vertical distribution of soil moisture. However, significant discrepancies still exist in the model based

326 on comparisons with observed data. The discrepancies may be associated with uncertainties in
327 soil-related physical parameters, such as a few that we listed in the earlier sections. For example, a
328 wide range of values have been reported in the literature for the parameter V_s . In the above
329 simulations, we assigned $V_s = 10^{-4} \text{ m s}^{-1}$, which is probably at the low end of the documented values.
330 An additional simulation was performed using a 10-fold higher V_s value (i.e., $V_s = 10^{-3} \text{ m s}^{-1}$), and the
331 resulting soil moisture changes were similar to those presented in Figs. 5 and 6 with differences of only
332 a few percent and thus are barely legible in Figs. 9 and 10. When a smaller value of $V_s = 10^{-5} \text{ m s}^{-1}$
333 was used, the effect of stem-root flow on soil moisture was similar but the magnitude of the changes
334 was reduced by approximately 50%. These sensitivity tests give an indication of the uncertainties
335 associated with V_s .

336 Even with the maximum V_s , the simulated soil moistures at the bottom layer are still lower than
337 observed. More realistic values for other soil physical parameters and/or optimizations of these
338 parameters are required. Xue et al. (1996) pointed out that land surface models such as SSiB are quite
339 sensitive to soil-type dependent parameters such as the hydraulic conductivity at saturation and the
340 coefficient used to calculate soil water potential. Such parameters can vary significantly from place
341 to place, and sufficient information to assign appropriate values is usually lacking. This is
342 particularly true for LHC where the soil types exhibited a rather inhomogeneous vertical distribution,
343 and some humus layers could exist to retard surface drainage. Another critical issue is the treatment
344 of water flow across the bottom soil layer. In our current model, soil moisture can leave the bottom

刪除: 4

刪除: 5

刪除: 8

刪除: 9

349 layer with a fixed efficiency, but no recharge from the water table below is allowed. These issues
350 might cause the model to underestimate the soil moisture in the bottom layer (regardless of the
351 presence of stem-root flow), which occurred in both the LHC and HAPEX simulations (cf. Figs. 5c
352 and 6c). On the other hand, the overestimation of soil moisture in SM1 and the underestimation in
353 SM3 in spring at LHC (Fig. 5) could also be explained by missing mechanisms such as hydraulic
354 redistribution (cf. Brooks et al., 2002), which provides a bypass of soil moisture through the inside of
355 the root rather than the exterior surface of the root as in the case of stem-root flow transport. On the
356 other hand, the overestimation of the middle-layer soil moisture at HAPEX may be partly
357 contributed from the plant uptake process which was not considered in this study. Besides, due to a
358 lack of observational data, we used a uniform vertical distribution of root, which might be the other
359 issue on different effects on two sites from stem-root flow. In recent years, U.S. Department of
360 Energy has supported a number of projects to measure the root vertical distribution. With more
361 data becoming available, we should be able to more realistically assess its effects. Henderson-Sellers
362 (1996) indicated that a full evaluation of land surface model's simulation against observations can be
363 established only when the initial conditions and all soil parameters are known precisely. Because
364 this study lacks of process-level data, so the improvement should be more prudent to represent.
365 Since this exploratory study focuses on introducing the stem-root flow mechanisms in a land surface
366 model and test its possible impact, we will not further test the uncertainty due to other parameters in
367 this paper. We hope more relevant measurements (such as the root distribution, stemflow to leaf

刪除: 4

刪除: 5

刪除: 4

371 drainage ratio, and root flow velocity) will provide useful information to study these issues further.

372

373 6. Conclusion

374 In this study, a stem-root flow mechanism, which provides an efficient water channel for rain to

375 penetrate into deep soil, was formulated and implemented into an offline version of the SSiB

376 land-atmosphere model. The model was used to simulate soil moisture variation at two sites with

377 different climate and ecology conditions: LHC with a mountain rainforest climate and HAPEX with a

378 Mediterranean climate. The results showed that the inclusion of the stem-root flow mechanism

379 substantially improved the capability of the model to simulate vertical soil moisture profiles.

380 Stem-root flow generally caused a drying of the top soil layer (upper 20 cm) and a moistening of the

381 bottom layer (below 50 cm) in the model. On a few occasions, such as after a long dry period, the

382 surface layer may be less dry than without the stem-root flow due to greater water supply from the

383 lower layers. The middle soil layer at LHC was also moistened and, in many instances during rainfall

384 events, the moisture in this layer fluctuated more intensely than in the top layer in response to the

385 stem-root flow. However, in the HAPEX case, the middle layer became dryer with less fluctuation.

386 Due to differences in plant and soil types, the strength of the stem-root flow was greater at LHC than at

387 HAPEX.

388 The change in soil moisture associated with the stem-root flow leads to significant modifications

389 in heat and moisture fluxes between the land and atmosphere. The general drying of the surface soil

390 leads to reduced soil evaporation and thus increased soil temperature. Plant transpiration at LHC was
391 not significantly affected by the stem flow because the soil moisture content was maintained well
392 above the wilting point. Therefore, the stem-root flow related to energy flux between the soil and
393 atmosphere is mainly controlled by sensible heat. In this sense, LHC may be considered as having an
394 energy-limited evapotranspiration regime. In contrast, the HAPEX soil (especially the top layer) was
395 generally dryer and sometimes fell below the wilting point. Plant transpiration can thus be
396 substantially affected by the stem-root flow. Changes in transpiration lead to changes in air
397 temperature, which, in turn, influence soil temperature. This effect is stronger than that resulting from
398 the soil evaporation associated with changes in the soil moisture of the top soil layer. At the HAPEX
399 site, evapotranspiration was more soil moisture-limited than energy-limited, and its net change in heat
400 flux associated with the stem-root flow was dominated by latent heat. While the stem-root flow effect
401 on soil moisture was weaker there than at LHC, the energy flux exchanges were actually stronger due
402 to the sensitive transpiration process.

403 Through the impact on soil moisture profiles, stem-root flow can significantly affect evaporation
404 and transpiration processes. The associated changes in moisture and energy fluxes between the land
405 and atmosphere may affect boundary-layer stability and convective processes. As evapotranspiration
406 returns as much as 60% of the precipitation back to the atmosphere over land (Oki and Kanae, 2006),
407 the stem-root flow mechanism may be a key factor in controlling the surface water budget and
408 hydrological cycle. The enhanced storage of water in deep soil layers may have a long-term effect on

409 the climate system. These issues are worthy of further investigation through more relevant
410 observations and testing by coupling the stem-root flow mechanism with global climate models.

411

412 **Acknowledgment:** This study was supported by the Ministry of Science and Technology of the
413 Republic of China on Taiwan through project MOST-100-2119-M-002-023-MY5. Dr. Y. Xue's

刪除: NSC-100-2119-M-002-023-
MY5

414 support is from U.S. NSF AGS-1346813. We are also grateful to Dr. S. Sun for technical assistance
415 on SSiB, Drs. M.-H. Li and Y.-Y. Chen for providing observation data, Dr. W.-L. Liang for helpful
416 suggestions, and the National Center for High-performance Computing for computer time and
417 facilities. We also deeply appreciate three reviewers' efforts to provide insightful and constructive
418 comments and suggestions to improve and revise the paper.

刪除: and

格式化: 字型: (中文) + 本文中文字
型 (新細明體)

419

420 **Appendix.** Derivation of D_{eff}

421 The parameter D_{eff} in Eq. (4) was derived in a similar fashion as in Zimmerman and Bodvarsson
422 (1991). As shown in Fig. A1, the part of soil next to the root flow absorbs water and form a thin,
423 saturated boundary of width λ . A gradient of soil moisture is formed in the transition zone (of
424 width δ), with soil water potential decrease from the saturated state, Ψ_s , to that of the bulk soil, Ψ_w .
425 Diffusion of soil moisture toward the bulk soil is directly proportional to this gradient.

426 The soil moisture horizontal (x -direction) movement can be express as following:

$$427 \rho \frac{\partial \theta}{\partial t} = \frac{\partial}{\partial x} \left[K(\Psi) \frac{\partial \Psi}{\partial x} \right] \quad (\text{A1})$$

431 where ρ is soil porosity; θ is the ratio of soil moisture content to its saturated state; K (in m s^{-1}) is the
 432 hydraulic conductivity of the soil; and Ψ (in m) is the soil water potential. Equation (A1) is subject
 433 to the following initial and boundary conditions:

434 $\theta(0, t) = 1, \theta(x, 0) = \theta_w, \theta(x \rightarrow \infty, t) = \theta_w .$ (A2)

435 The first condition means that, when the root-flow occurs, soil at the root-soil interface ($x = 0$) is
 436 saturated. The next two conditions specify the initial bulk soil moisture content, θ_w , and this value
 437 remains unaffected by the root flow at a far distance from the root-soil interface throughout the
 438 integration time period.

439 The hydraulic conductivity and water potential of the soil can be represented with the empirical
 440 relationship of Clapp and Hornberger (1978):

441 $K(\Psi) = K_s(\Psi / \Psi_s)^{-\frac{3}{b}+2}$ (A3)

442 $\Psi = -\Psi_s \theta^b ,$ (A4)

443 where K_s (in m s^{-1}) is hydraulic conductivity at saturation; b is an empirical constant dependent on
 444 the soil type. By introducing a similarity variable η and two normalized variables $\hat{\Psi}$ and \hat{K} :

445 $\eta \equiv \sqrt{\frac{\rho}{K_s \Psi_s t}}, \hat{\Psi} \equiv \frac{\Psi}{\Psi_s}, \text{ and } \hat{K} \equiv \frac{K}{K_s},$ (A5)

446 Eq. (A1) can be transformed into

447 $\frac{d}{d\eta} \left(\hat{K}(\hat{\Psi}) \frac{d\hat{\Psi}}{d\eta} \right) + \frac{\eta}{2} \frac{d\theta}{d\eta} = 0,$ (A6)

448 whereas the initial and boundary conditions in Eq. (A2) reduced to

449 $\theta(0) = 1, \theta(\eta \rightarrow \infty) = \theta_w$ (A7)

450 Zimmerman and Bodvarsson (1991) showed that the solution for Eq. (A6) with conditions in Eq. (A7)

451 can be approximated as:

$$452 \quad \begin{cases} \theta = 1, & \text{if } 0 \leq \eta \leq \lambda \\ \theta = 1 - (1 - \theta_w) \frac{\eta - \lambda}{\delta}, & \text{if } \lambda < \eta \leq \lambda + \delta \\ \theta = \theta_w, & \text{if } \lambda + \delta < \eta < \infty \end{cases} \quad (A8)$$

453 where

$$454 \quad \delta = 2 \sqrt{\frac{b}{1 + \frac{b}{2} \frac{2}{b(1 - \theta_w)}}} \quad \text{and} \quad \lambda = \frac{\delta}{b(1 - \theta_w)} \quad (A9)$$

455 That is, within the root-soil boundary ($0 \leq \eta \leq \lambda$), θ is saturated (=1); whereas in the transition zone

456 ($\lambda < \eta \leq \lambda + \delta$), θ decreases linearly from 1 to θ_w . Here, δ is the “effective thickness” of

457 diffusion in the η coordinate, and it can be revert back to the x coordinate using the similarity

458 conversion in Eq. (A5):

$$459 \quad D_{\text{eff}} = \delta \sqrt{\frac{K_s \Psi_s t}{\rho}} \quad (A10)$$

460 By applying the actual rainfall duration for t into Eq. (A10), we calculated the mean values of $D_{\text{eff}} =$

461 0.005 m for the HAPEX site and $D_{\text{eff}} = 0.03$ m for the LHC site.

462

463 **Reference**

464 André, F., Jonard, M., and Ponette, Q.: Influence of species and rain event characteristics on
465 stemflow volume in a temperate mixed oak-beech stand, *Hydrological Processes*, 22,
466 4455-4466, 10.1002/hyp.7048, 2008.

467 Angevine, W. M., Bazile, E., Legain, D., and Pino, D.: Land surface spinup for episodic modeling,
468 *Atmos. Chem. Phys.*, 14, 8165-8172, 2014.

469 Beven, K., and Germann, P.: Macropores and water flow in soils, *Water Resources Research*, 18,
470 1311-1325, 1982.

471 Böhm, W.: *Methods of studying root systems*, Springer-Verlag, 1979.

472 Boone, A. and Wetzel, P. J.: Issues related to low resolution modeling of soil moisture: experience
473 with the PLACE model, *Global and Planetary Change*, 13, 161-181, 1996.

474 Brooks, J. R, Meinzer, F. C., Coulombe, R. and Gregg, J.: Hydraulic redistribution of soil water during
475 summer drought in two contrasting Pacific Northwest coniferous forests. *Tree Physiology*, 22,
476 1107-1117, 2002

477 Budyko, M. I.: *Climate and Life*, Academic Press, New York, 1974.

478 Chase, T. N., Pielke, R. A., Kittel, T. G. F., Nemani, R., and Running, S. W.: Sensitivity of a general
479 circulation model to global changes in leaf area index, *Journal of Geophysical Research: Atmospheres*, 101, 7393-7408, 1996.

480 Chase, T. N., Pielke Sr, R. A., Kittel, T. G. F., Nemani, R. R., and Running, S. W.: Simulated impacts
481 of historical land cover changes on global climate in northern winter, *Climate Dynamics*, 16,
482 93-105, 2000.

483 Chen, Y.-Y.: *Investigating the Seasonal Variability of Surface Heat and Water Vapor Fluxes with
484 Eddy Covariance Techniques: a Subtropical Evergreen Forest as an Example*, Doctoral,
485 Graduate Institute of Hydrological and Oceanic Sciences, National Central University, 149 pp.,
486 2012.

487 Clapp, R.B. and Homberger, G.M.: Empirical equations for some soil hydraulic properties, *Water
488 Resour. Res.*, 14: 601-604, 1978.

489 de Goncalves, L. G. G., Shuttleworth, W. J., Burke, E. J. , Houser, P., Toll, D. L., Rodell, M. and
490 Arsenault, K.: Toward a South America Land Data Assimilation System: Aspects of land
491 surface model spin-up using the Simplified Simple Biosphere, *J. Geophys. Res.*, 111,
492 D17110, 2006.

493 Dorman, J. L., and Sellers, P. J.: A Global climatology of albedo, roughness length and stomatal

495 resistance for atmospheric general circulation models as represented by the Simple Biosphere
496 Model (SiB), *Journal of Applied Meteorology*, 28, 833-855, 1989.

497 Gerke, H.: Bypass flow in soil, in: *Encyclopedia of Agrophysics*, edited by: Gliński, J., Horabik, J.,
498 and Lipiec, J., *Encyclopedia of Earth Sciences Series*, Springer Netherlands, 100-105, 2014.

499 Good, S. P., Noone, D., and Bowen, G.: Hydrologic connectivity constrains partitioning of global
500 terrestrial water fluxes, *Science*, 349(6244), 175–177, 2015.

501 Goutorbe, J.-P., J. Noilhan, C. Valancogne, and Cuenca, R. H.: Soil moisture variations during
502 HAPEX-MOBILHY, *Annals of Geophysics*, 7, 415-426, 1989.

503 Goutorbe, J. P.: A Critical assessment of the Samer network accuracy, in: *Land Surface Evaporation*,
504 edited by: Schmugge, T., and André, J.-C., Springer New York, 171-182, 1991.

505 Goutorbe, J. P., and Tarrieu, C.: HAPEX-MOBILHY data base, in: *Land Surface Evaporation*, edited
506 by: Schmugge, T., and André, J.-C., Springer New York, 403-410, 1991.

507 Henderson-Sellers, A., Pitman, A. J., Love, P. K., Iraennejad, P. and Chen, T. H.: The Project for
508 Intercomparison of Land Surface Parameterization Schemes (PILPS): Phases 2 and 3. *Bull.*
509 *Amer. Meteor. Soc.*, 76, 489-503, 1995

510 Henderson-Sellers, A.: Soil moisture simulation: Achievements of the RICE and PILPS
511 intercomparison workshop and future directions. *Global Planet. Chang.*, 13, Issues 1–4,
512 99-115, 1996

513 Jarvis, N. J., and Dubus, I. G.: State-of-the-art review on preferential flow, www.eu-footprint.org, 60
514 pp., 2006.

515 Jasechko, S., Sharp, Z. D., Gibson, J. J., Birks, S. J., Yi, Y. and Fawcett, P. J.: Terrestrial water fluxes
516 dominated by transpiration, *Nature*, 496(7445), 2013.

517 Johnson, M. S., and Lehmann, J.: Double-funneling of trees: stemflow and root-induced preferential
518 flow, *Ecoscience*, 13, 324-333, 2006.

519 Köhne, J. M., Köhne, S., and Šimůnek, J.: A review of model applications for structured soils: a)
520 Water flow and tracer transport, *Journal of Contaminant Hydrology*, 104, 4-35, 2009.

521 Levia, D. F., and Frost, E. E.: A review and evaluation of stemflow literature in the hydrological and
522 biochemical cycles of forested and agricultural ecosystems., *Journal of Hydrology*, 274, 1-29,
523 2003.

524 Levia, D. F., and Germer, S.: A review of stemflow generation dynamics and stemflow-environment
525 interactions in forests and shrublands, *Rev. Geophys.*, 53, 673–714, 2015.

526 Li, J., He, B., Chen, Y., Huang, R., Tao, J., and Tian, T.: Root distribution features of typical herb
527 plants for slope protection and their effects on soil shear strength, *Transactions of the Chinese
528 Society of Agricultural Engineering*, 29, 144-152, 2013.

529 Li, X.-Y., Yang, Z.-P., Li, Y.-T., and Lin, H.: Connecting ecohydrology and hydropedology in desert
530 shrubs: stemflow as a source of preferential flow in soils, *Hydrology and Earth System
531 Sciences*, 13, 1133-1144,2009.

532 Li, X.-Y., Lin, H., and Levia, D. F.: Coupling ecohydrology and hydropedology at different
533 spatio-temporal scales in water-limited ecosystems, in: *Hydropedology*, edited by: Lin, H.,
534 Academic Press, Boston, 737-758, 2012.

535 Liang, W.-L., Kosugi, K. i., and Mizuyama, T.: Heterogeneous soil water dynamics around a tree
536 growing on a steep hillslope, *Vadose Zone J.*, 6, 879-889, 2007.

537 Liang, W.-L., Kosugi, K. i., and Mizuyama, T.: A three-dimensional model of the effect of stemflow
538 on soil water dynamics around a tree on a hillslope. *J. Hydro.*, 366(1-4), 62-75, 2009.

539 Lim, Y.- J., Hong, J., Lee, T.-Y.: Spin-up behavior of soil moisture content over East Asia in a land
540 surface model, *Meteorology and Atmospheric Physics*, 118(3), 151-161, 2012.

541 Liu, I.-W. Y., Waldron, L. J., and Wong, S. T. S.: Application of nuclear magnetic resonance imaging
542 to study preferential water flow through root channels, *Tomography of Soil-Water-Root
543 Processes*, 135-148, 1994.

544 McGuffie, K., Henderson-Sellers, A., Zhang, H., Durbidge, T. B., and Pitman, A. J.: Global climate
545 sensitivity to tropical deforestation, *Global and Planetary Change*, 10, 97-128, 1995.

546 Návar, J.: The causes of stemflow variation in three semi-arid growing species of northeastern

547 Mexico, Journal of Hydrology, 145, 175-190, 1993.

548 Neave, M., and Abrahams, A. D.: Vegetation influences on water yields from grassland and
549 shrubland ecosystems in the Chihuahuan Desert, Earth Surface Processes and Landforms, 27,
550 2002.

551 Oki, T. and Kanae, S.: Global Hydrological Cycles and World Water Resources. *Science*, **313**,
552 1068-1072, 2006.

553 Sellers, P. J., Mintz, Y., Sud, Y. C., and Dalcher, A.: A Simple Biosphere Model (SIB) for use within
554 general circulation models, *Journal of the Atmospheric Sciences*, 43, 505-531, 1986.

555 Seneviratne, S. I., Corti, T., Davin, E. L., Hirschi, M., Jaeger, E. B., Lehner, I., Orlowsky, B., and
556 Teuling, A. J.: Investigating soil moisture–climate interactions in a changing climate: A review,
557 *Earth-Science Reviews*, 99, 125-161, 2010.

558 Shao, Y., Anne, R. D., Henderson-Sellers, A., Irannejad, P., Thorton, P., Liang, X., Chen, T. H., Ciret,
559 C., Desborough, C., Barachova, O., Haxeltine, A. and Ducharne, A.: Soil Moisture Simulation,
560 A report of the RICE and PILPS Workshop. GEWEX Tech. Note, IGPO Publ. Ser., 14, 179 pp,
561 1995.

562 Siegert, C. M., and Levia, D. F.: Seasonal and meteorological effects on differential stemflow
563 funneling ratios for two deciduous tree species, *Journal of Hydrology*, 519, Part A, 446-454,
564 2014.

565 Tanaka, T., Taniguchi, M., and Tsujimura, M.: Significance of stemflow in groundwater recharge. 2:
566 A cylindrical infiltration model for evaluating the stemflow contribution to groundwater
567 recharge, *Hydrological Processes*, 10, 81-88, 1996.

568 Taniguchi, M., Tsujimura, M., and Tanaka, T.: Significance of stemflow in groundwater recharge. 1:
569 Evaluation of the stemflow contribution to recharge using a mass balance approach,
570 *Hydrological Processes*, 10, 71-80, 1996.

571 Wei, Z., Yoshimura, K., Okazaki, A., Kim, W., Liu, Z., and Yokoi, M.: Partitioning of
572 evapotranspiration using high-frequency water vapor isotopic measurement over a rice paddy

573 field, Water Resources Research, 51, 3716–3729, 2015.

574 Wu, B.-Y.: Simulations of Land Surface Fluxes of the Lien Hua Chih Experimental Watershed with
575 Land Process Models, Master, Graduate Institute of Hydrological and Oceanic Sciences,
576 National Central University, 100 pp., 2011.

577 Xue, Y., Sellers, P., Kinter, J., and Shukla, J.: A simplified biosphere model for global climate studies.
578 *J. Climate*, 4, 345-364, 1991.

579 Xue, Y., Zeng, F. J., and Adam Schlosser, C.: SSiB and its sensitivity to soil properties—a case study
580 using HAPEX-Mobilhy data, *Global and Planetary Change*, 13, 183-194, 1996.

581 Yang, Y., Uddstrom, M., and Duncan, M.: Effects of short spin-up periods on soil moisture
582 simulation and the causes over New Zealand, *J. Geophys. Res.*, 116, D24108.

583 Zhang, Y.-Q., Q. K. Zhu, and Qi, S.: Root system distribution characteristics of plants on the terrace
584 banks and their impact on soil moisture, *Acta Ecologica Sinica*, 25, 500-506, 2005.

585 Zhao, M., Pitman, A. J., and Chase, T.: The impact of land cover change on the atmospheric
586 circulation, *Climate Dynamics*, 17, 467-477, 2001.

587 Zimmerman, R. and Bodvarsson, G.: A simple approximate solution for horizontal infiltration in a
588 Brooks-Corey medium. *Transport in Porous Media*, 6, 195-205, 1991.

589

590

591

592 Table 1. Basic parameters used for describing the LHC and HAPEX sites. LHC data were obtained
 593 from Wu (2011); HAPEX data were obtained from Goutorbe et al. (1989).

Location	LHC	HAPEX
Annual rainfall	2317 mm	856 mm
Mean temperature	19.7°C	8.6°C
Altitude	770 m	113 m
Vegetation cover	Rainforest of mixed evergreens and hardwoods	Soya crop
Soil type	Loam	17% clay content, 46% silt, 37% sand
Soil moisture measurement depth	10, 30, 50, 70, 90 cm	Every 10 cm down to 160 cm
Soil wetness exponent	2.5	5.66
Soil tension at saturation	-0.1 m	-0.30 m
Hydraulic conductivity at saturation	$1 \times 10^{-6} \text{ m s}^{-1}$	$4 \times 10^{-6} \text{ m s}^{-1}$
Soil porosity	0.530	0.446
Slope	0.55	0.05

594

595

596 Table 2. Monthly leaf area index values (in $\text{m}^2 \text{ m}^{-2}$) for LHC in 2010 and HAPEX in 1986. LHC
 597 data were obtained from Wu (2011); HAPEX data were obtained from Goutorbe et al. (1989).

Month	1	2	3	4	5	6	7	8	9	10	11	12
LHC	3.34	3.08	3.06	3.04	4.35	4.77	4.84	4.91	4.66	4.4	4.2	4.25
HAPEX	0	0	0	0	1	3	3	3	3	0	0	0

598

599

600

601 Table 3. The mean bias, root-mean-square error (RMSE), and standard deviation (STD) in simulated
 602 soil moisture comparing to observations (obs). “Control” stands for simulations without the
 603 stem-root flow mechanism, and “SLR90%” or “SLR50%” are simulations with the optimal stemflow
 604 to leaf drainage ratio. Unit: $\text{m}^3 \text{ m}^{-3}$

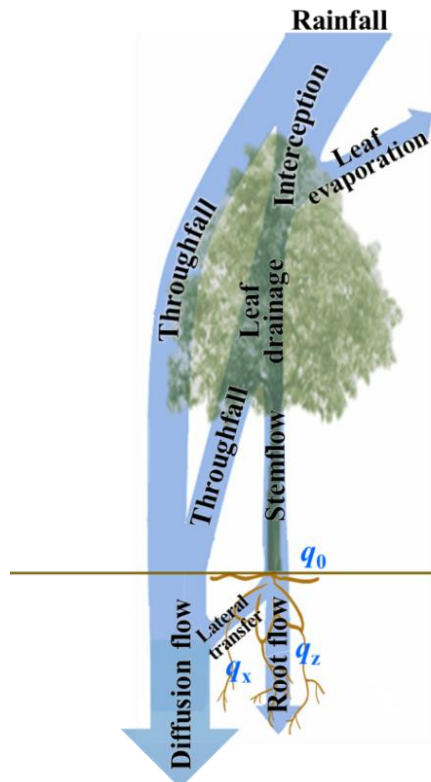
	SM1			SM2			SM3		
	bias	RMSE	STD	bias	RMSE	STD	bias	RMSE	STD
LHC control-obs	-0.003	0.142	0.142	-0.098	0.153	0.012	-0.141	0.193	0.131
LHC SLR90%-obs	0.023	0.056	0.051	-0.034	0.050	0.036	-0.038	0.048	0.029
HAPEX control-obs	0.018	0.036	0.032	0.032	0.037	0.019	-0.057	0.085	0.063
HAPEX SLR50%-obs	0.009	0.030	0.029	0.024	0.030	0.018	-0.049	0.074	0.056

605

606

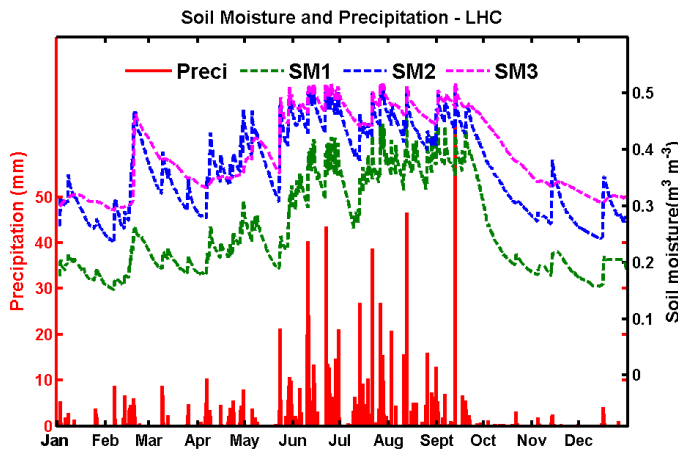
607 Table 4. Mean and maximum changes in daily temperatures and energy fluxes due to the stem-root
 608 flow (between optimal SLR run and control run) during the growing season. Canopy air temperature
 609 (T_C), soil surface temperature (T_S) and leaf temperature (T_L) are in $^{\circ}\text{C}$; Transpiration (TR), soil
 610 evaporation (SE), leaf evaporation (LE), sensible heat (SH) and latent heat (LH) are in W m^{-2} .

	ΔT_C	ΔT_S	ΔT_L	ΔTR	ΔSE	ΔLE	ΔSH	ΔLH
LHC mean	0.32	0.31	0.34	0.20	-1.19	0.31	2.02	-0.68
LHC maximum	2.90	2.59	3.18	1.01	-15.50	11.34	31.44	-16.81
HAPEX mean	0.04	0.11	0.03	1.06	-2.17	0.28	0.52	-0.82
HAPEX maximum	1.27	1.63	1.70	-66.74	-19.5	9.95	51.16	-66.29



614
615 Figure 1. Stem-root flow conceptual diagram. Leaf drainage in the model can be separated into
616 throughfall and stemflow. Following the stemflow path, rainwater can continue via the root system to
617 reach deep soil layers and the water table. The stemflow that reaches the soil top, q_0 , is divided into a
618 downward transfer flux (i.e., the root flow) q_z and a lateral transfer flux q_x (from the root surface to the
619 soil), and the two transfer fluxes regulate the root flow thickness.

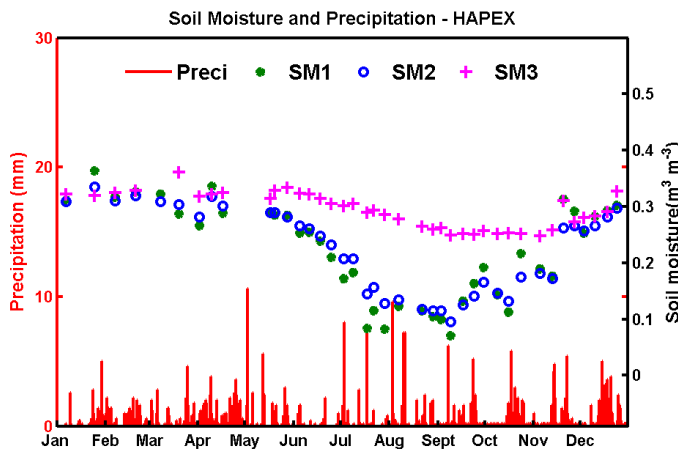
620



621

622 Figure 2. The hourly soil moisture (curves, right axis) and precipitation (red bars, left axis) observed
 623 at LHC during 2010. SM1, SM2 and SM3 represent soil moisture at 10 cm (green-dashed curve), 40
 624 cm (blue-dashed curve; average of 30 cm and 50 cm observations) and 90 cm (magenta-dashed curve),
 625 respectively.

626

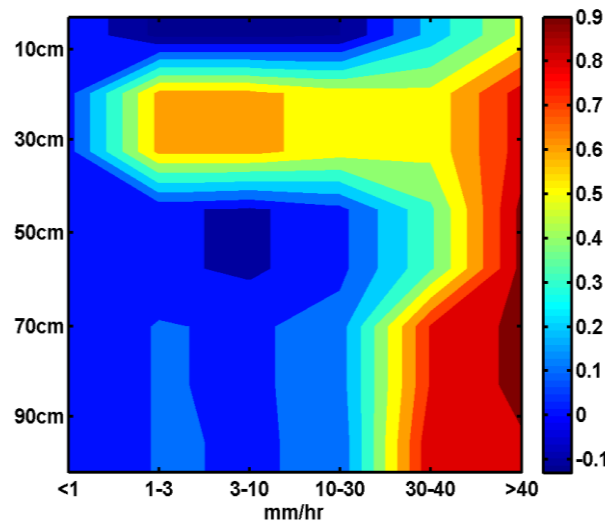


627

628 Figure 3. The weekly soil moisture (symbols, right axis) and hourly precipitation (red bars, left axis)
 629 observed at HAPEX during 1986. SM1 SM2 and SM3 represent the mean soil moisture in the 0–20
 630 cm (green dot), 20–50 cm (blue circle), and 50–160 cm (magenta cross) layers, respectively.

631

632



633

634

635

636

637

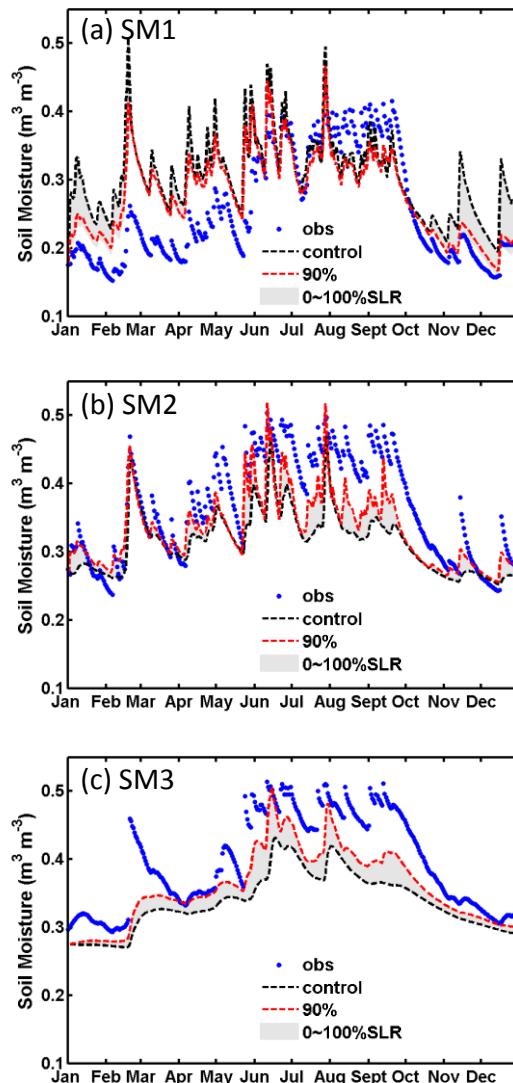
Figure 4: Correlation between hourly changes in precipitation and soil moisture at the Lien-Hua Chih

格式化: 靠左

station in 2010. The ordinate is the soil depth and the abscissa is the rainfall intensity. Color

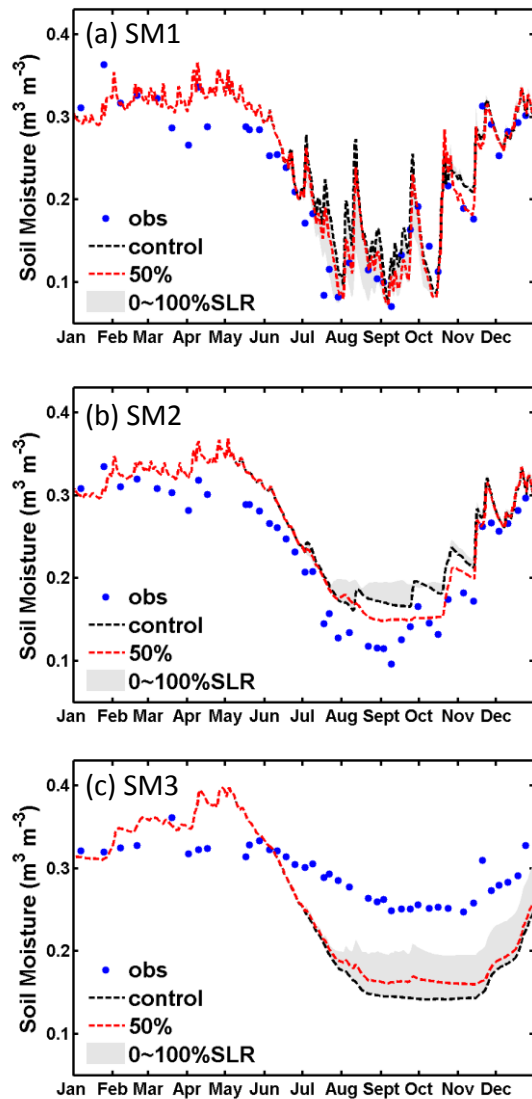
格式化: 字型: (中文) + 本文中文字型 (新細明體)

shading indicates the correlation coefficient with values shown in the color bar to the right.



640 | Figure 5. Simulated and observed soil moisture for the LHC site at depths of (a) SM1 (0-20 cm), (b)
641 | SM2 (20-70 cm), and (c) SM3 (70-170 cm). Observed results are shown as blue dots. Simulations
642 | with SLR=0 (i.e., control run, without stem-root flow) and SLR=90% are shown as black-dashed and
643 | red-dashed curves, respectively. The area of grey shading enclosed by SLR=0% and 100% indicates
644 | the possible range of the stem-root flow effects. All simulation results are daily averages.

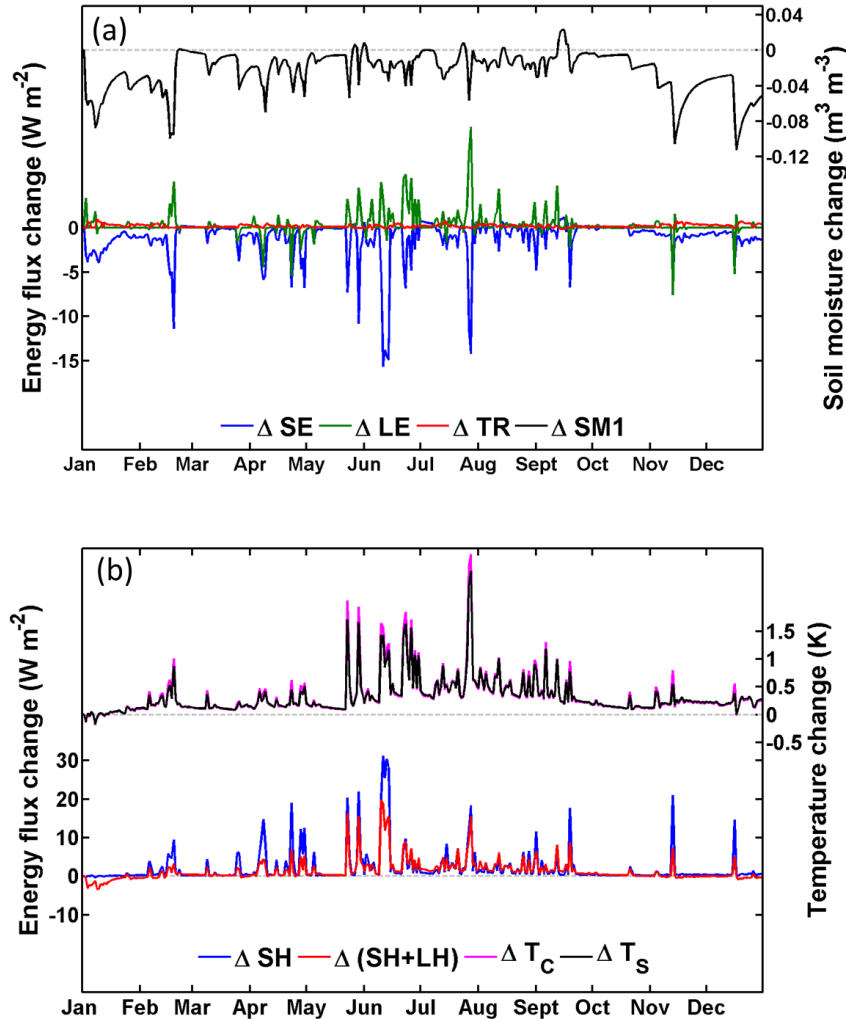
刪除: 4



647
648 | Figure 6. Same as Fig. 5, but for the HAPEX case at depths of (a) SM1 (0-20 cm), (b) SM2 (20-50
649 cm), and (c) SM3 (50-160 cm). Red-dashed curves are results with SLR=50%.

刪除: 5

刪除: 4



654
655 | Figure 7. Difference in daily mean heat fluxes and soil moisture due to stem-root flow at the LHC
656 case. (a) Changes in soil evaporation (SE; blue curve), leaf evaporation (LE; green curve),
657 transpiration (TR; red curve) and soil moisture of the surface layer (SM1; black curve; right axis); (b)
658 Changes in sensible heat (SH; blue curve), total heat (sensible heat plus latent heat (SH+LH); red
659 curve), canopy air temperature (T_c; magenta curve; right axis) and soil temperature (T_s; black curve;
660 right axis). Grey dashed lines indicate the zero baseline.

刪除: 6

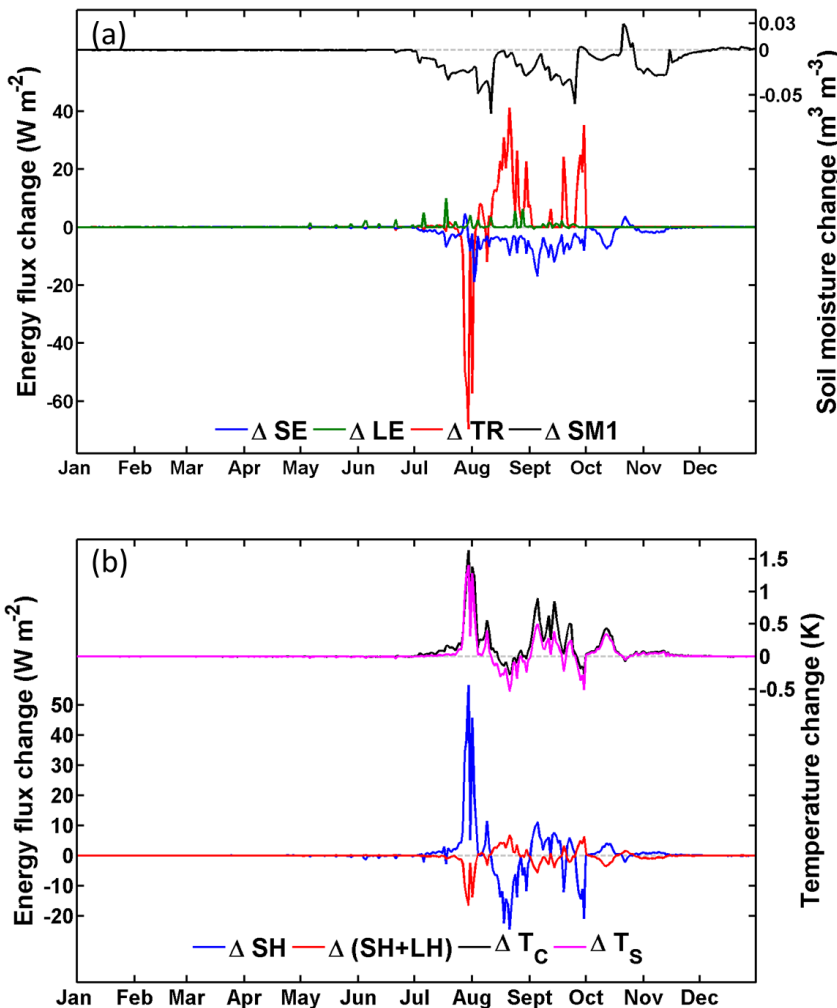


Figure 8. Same as Fig. 7, but for the HAPEX case.

刪除: 7

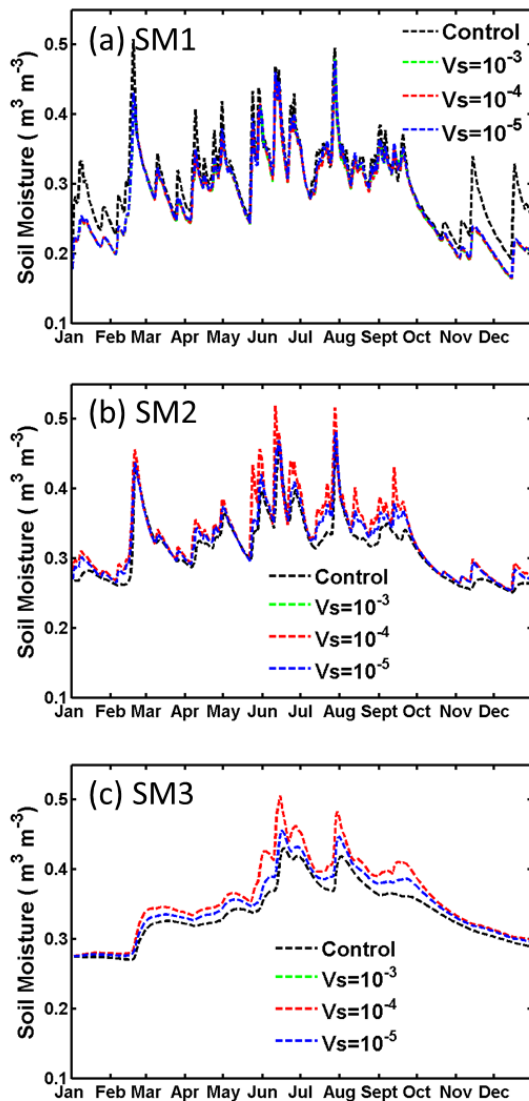
刪除: 6

663

664

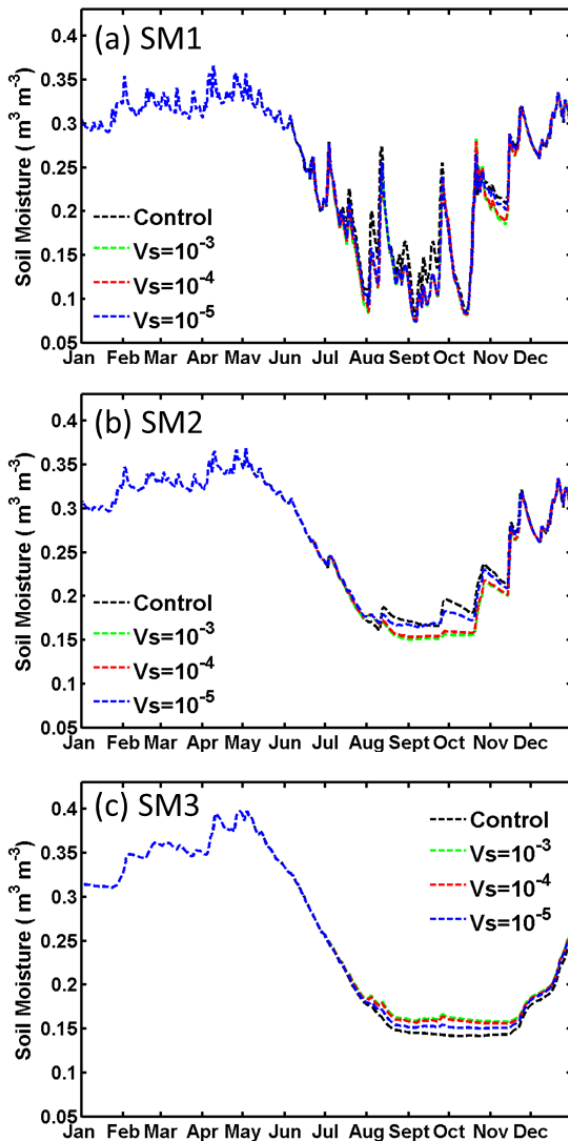
665

666



669
670 | Figure 9. Sensitivity test on V_s for the LHC case with optimal SLR=90% at depths of (a) SM1 (0-20
671 cm), (b) SM2 (20-70 cm), and (c) SM3 (70-170 cm). The green-dashed, red-dashed and blue-dashed
672 curves are for $V_s = 10^{-3}$, 10^{-4} , and 10^{-5} m s^{-1} , respectively. Also shown in black-dashed curves are the
673 control run results (i.e., SLR=0).

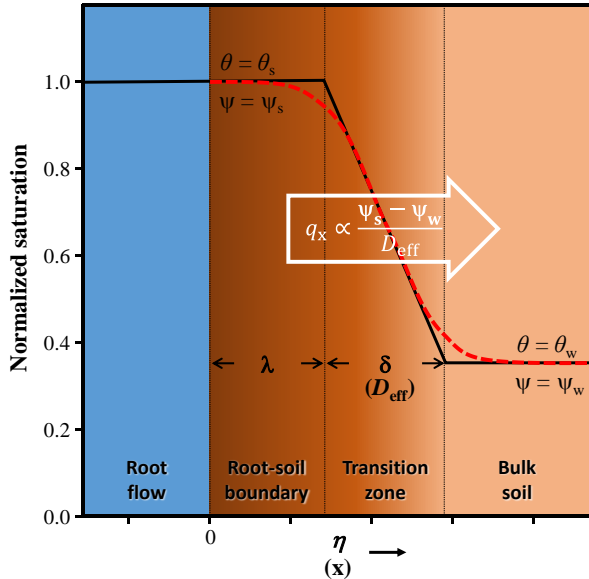
刪除: 8



676
677 | Figure 10. Same as Fig. 9, but SLR=50% for the HAPEX case at depths of (a) SM1 (0-20 cm), (b)
678 SM2 (20-50 cm), and (c) SM3 (50-160 cm).

刪除: 9

刪除: 8



682

683 Figure A1. Schematics of the root flow-soil boundary and soil moisture transition for the
 684 parameterization of horizontal water flux q_x . The red-dashed line represents the analytical solution,
 685 and the black-solid line represents the parameterization. Soil moisture is saturated ($=\theta_s$) in the
 686 root-soil boundary (width λ), and decreases linearly in the transition zone (width δ) before reaching
 687 that of the bulk soil (θ_w).